International Journal of Nanomedicine

Dovepress
open access to scientific and medical research

Open Access Full Text Article

ORIGINAL RESEARCH

Creation of Bony Microenvironment with Extracellular Matrix Doped-Bioactive Ceramics to Enhance Osteoblast Behavior and Delivery of Aspartic Acid-Modified BMP-2 Peptides

This article was published in the following Dove Press journal:
International Journal of Nanomedicine

International Journal of Nanomedicine downloaded from https://www.dovepress.com/
For personal use only.

Jinge Zhou[1,*]
Zekang Xiong[1,*]
Man Liu[2]
Liang Yang[1]
Sheng Yao[1]
Kaifang Chen[1]
Keda Yu[1]
Yanzhen Qu[1]
Tingfang Sun[1]
Xiaodong Guo[1]

[1]Department of Orthopaedics, Union Hospital, Tongji Medical College, Huazhong University of Science and Technology, Wuhan 430022, People's Republic of China; [2]Department of Gastroenterology and Hepatology, Taikang Tongji Hospital, Wuhan 430050, People's Republic of China

*These authors contributed equally to this work

Introduction: Decellularized matrix from porcine small intestinal submucosa (SIS) endows scaffolds with an ECM-like surface, which enhances stem cell self-renewal, proliferation, and differentiation. Mesoporous bioactive glass (MBG) is extensively recognized as an excellent bio-ceramic for fabricating bone grafts.

Materials and Methods: In the current study, SIS was doped on an MBG scaffold (MBG/SIS) using polyurethane foam templating and polydopamine chemistry method. To mimic the bony environment of a natural bone matrix, an ECM-inspired delivery system was constructed by coupling the BMP2-related peptide P28 to a heparinized MBG/SIS scaffold (MBG/SIS-H-P28). The release of P28 from MBG/SIS-H-P28 and its effects on the proliferation, viability, and osteogenic differentiation of bone marrow stromal stem cells were investigated in vitro and in vivo.

Results: Our research indicated that the novel tissue-derived ECM scaffold MBG/SIS has a hierarchical and interconnected porous architecture, and superior biomechanical properties. MBG/SIS-H-P28 released P28 in a controlled manner, with the long-term release time of 40 d. The results of in vitro experiments showed improvements in cell proliferation, cell viability, alkaline phosphatase activity, and mRNA expression levels of osteogenesis-related genes (*Runx-2, OCN, OPN*, and *ALP*) compared to those of MBG/SIS or MBG/SIS-P28 and MBG/SIS-H-P28. The in vivo results demonstrated that MBG/SIS-H-P28 scaffolds evidently increased bone formation in rat calvarial critical-sized defect compared to that in controls.

Conclusion: MBG/SIS-H-P28 scaffolds show potential as ideal platforms for delivery of P28 and for providing a bony environment for bone regeneration.

Keywords: small intestinal submucosa, mesoporous bioactive glass, microenvironment, osteogenesis, BMP2-related peptide

Introduction

The treatment of bone defects, especially large bone defects caused by trauma, infections, tumors, or genetic malformations, remains problematic.[1] Therefore, a desirable tissue-inducing biomaterial that enables bone regeneration is considered to be urgently needed. Ideal osteoinductive biomaterial should exhibit properties such as bioactivity of osteogenesis and angiogenesis, compressive strength, porous architecture, and controllable drug-delivery ability, in order to satisfy the requirements of bone tissue engineering.[2–4]

Correspondence: Xiaodong Guo; Tingfang Sun
Tel +8615327216660; +8613554435801
Email xiaodongguo@hust.edu.cn; tingfangsun@163.com

submit your manuscript | www.dovepress.com
DovePress
http://doi.org/10.2147/IJN.S272571

© 2020 Zhou et al. This work is published and licensed by Dove Medical Press Limited. The full terms of this license are available at https://www.dovepress.com/terms.php and incorporate the Creative Commons Attribution – Non Commercial (unported, v3.0) License (http://creativecommons.org/licenses/by-nc/3.0/). By accessing the work you hereby accept the Terms. Non-commercial uses of the work are permitted without any further permission from Dove Medical Press Limited, provided the work is properly attributed. For permission for commercial use of this work, please see paragraphs 4.2 and 5 of our Terms (https://www.dovepress.com/terms.php).

Mesoporous bioactive glass (MBG), which has a highly ordered mesopore-channel structure with a pore size of 2–50 nm,[5] has attracted much attention because it possesses a unique set of features, such as enhanced bioactivity as well as ability to release ions (Si, Ca, and P) and drugs locally, which help elicit specific therapeutic effects, osteoconductivity, osteogenesis, angiogenesis, and antibacterial properties.[6–8] Unfortunately, MBG scaffolds are commonly prepared using lyophilization or other common methods that often result in unsatisfactory pore connectivity, poor mechanical stability, and undesirable biodegradability, which directly exert a negative effect on the application and therapeutic efficacy of the scaffolds.[9] Therefore, there is much demand to develop new methods for fabrication of MBG scaffolds. Polyurethane (PU) sponge templating method is recognized as an economical and convenient molding method for developing highly interconnected pore structures.[10] The current study used a PU sponge mold to construct a porous MBG scaffold with a hierarchical structure.

To achieve desirable superficial biology, several investigators coated scaffold surfaces with extracellular matrix (ECM) proteins, such as collagen, glycosaminoglycan, and fibronectin, or functional peptides.[11–13] However, they did not reproduce the complex environment of the natural ECM, which supports bone regeneration, due to simple composition or deficient architecture. ECM provides a dynamic and complex environment for determination of stem cell fate.[14] Surface modification with tissue-derived ECM shows great potential in recapturing the environment of natural ECM. Small intestine submucosa (SIS), prepared from the submucosal layer of porcine intestine, is an acellular, non-immunogenic, biodegradable, xenogeneic, collagen-based, naturally occurring collagenous ECM material.[15] SIS consists of ~90% collagen (mainly Type I) and a wide variety of cytokines, including vascular endothelial growth factor (VEGF) and basic fibroblast growth factor-2 (bFGF-2), which are associated with tissue remodeling of the body wall, ligaments, and blood vessels.[16–19] Previous studies conducted by us and other research groups have demonstrated that SIS-based biological scaffolds exhibit excellent capability for guiding bone regeneration.[20,21] As such, SIS was expected to be a coating modifier able to provide a bone-like matrix for MBG scaffolds.

In addition, bone repair and regeneration comprises a complex cascade of biological events involving not only ECM and bone forming cells, but also osteogenic growth factors.[22] Bone morphogenetic protein-2 (BMP2) is one of the most effective growth factors for accelerating non-union, fracture, and spinal fusion. However, BMP-2 is associated with some disadvantages, such as high production cost, transient bioactivity due to short half-life, and risks of ectopic bone formation and tumorigenesis due to off-target effects and inappropriate adipogenesis.[23–25] To overcome these drawbacks, a short peptide, P28 (S[PO4]DDDDDDDKIPKASSVPTELSAISTLYL, molecular weight: 3091.20), derived from the knuckle epitope of BMP2, was designed by our team in a previous study.[24] P28 has a short chain of seven aspartic acids (Ds) and one phosphorylated serine at the N-terminus, which shows well-documented affinity for hydroxyapatite (HA) and contributes to nucleation of apatite crystallization and mineralization.[26,27]

Growth factor delivery has been intensively investigated, yielding a large number of delivery systems. However, only a few studies have examined the use of tissue-derived ECM in combination with an engineered 3D scaffold to achieve sustained release of a bioactive peptide. Previous studies have indicated that ECM naturally binds growth factors because these factors participate in specific interactions with heparan sulfate proteoglycans of the ECM.[28] Therefore, modification of biomaterial matrices via heparin has been extensively used to improve the delivery of growth factors. In the present study, MBG/SIS scaffold matrices were enhanced with heparin in order to control the delivery of P28.

The release profile of P28 from MBG/SIS-heparin-P28 (MBG/SIS-H-P28) was investigated in vitro. We hypothesized that an ECM-inspired delivery system of MBG/SIS-H-P28 may facilitate local, sustained release of P28, and a combination of MBG/SIS and P28 may synergistically create a bony microenvironment for cell self-renewal, proliferation, and differentiation in vitro, and induce bone regeneration in vivo.

Materials and Methods

Fabrication of MBG/SIS, MBG/SIS-P28, MBG/SIS-H-P28 Scaffolds

MBG: Hierarchical MBG scaffolds (1×1×1 cm^3 for mechanical tests; 1×1×0.2 cm^3 for in vitro cell experiments; Ø5×2 mm for in vivo assessments) were fabricated using the PU foam templating method. MBG gel was prepared following procedures described previously.[29] Typically, 12 g of Pluronic P123 (Mw = 5800; Sigma-Aldrich,

USA), 20.1 g of tetraethyl orthosilicate (TEOS98%; Sigma-Aldrich, USA), 4.2 g of $Ca(NO_3)_2{\cdot}4H_2O$, 2.19 g of triethyl phosphate (TEP, 98%; Sigma-Aldrich, USA), and 1 g of 0.5 M HCl were dissolved in 180 g of ethanol (Si/Ca/P = 80:15:5, molar ratio) and stirred for 24 h. Afterwards, the PU sponges (40 ppi) were completely immersed in this solution until they were uniformly coated with the MBG gel. Following drying at 60°C for 48 h, the samples were calcined at 700°C (with heating rate of 1°C/min) for 5 h in a muffle furnace to obtain the MBG scaffolds. The mesopore-channel structures of the scaffolds were characterized through transmission electron microscopy (TEM) (Tecnai G2 20; FEI, Inc., the Netherlands).

MBG/SIS: SIS was immobilized on MBG scaffolds via the polydopamine (pDA)-assisted coating method.[30] SIS solution was prepared as previously described.[31] Dopamine hydrochloride (Sigma-Aldrich, USA) was added to Tris-HCl buffer solution (10.0 mM, pH 8.5) to obtain a dopamine solution (2.0 g/L). Subsequently, MBG scaffolds were immersed in the dopamine solution while stirring at room temperature for 12 h. Then, the MBG scaffolds were transferred into 0.5% SIS solution for 12 h at 37°C to ensure effective adhesion of SIS. The scaffolds were air dried in a fume hood for 1 d followed by freeze-drying for 1 d and sterilization with ethylene oxide.[31] The microstructure of the scaffolds was characterized via a scanning electron microscope (SEM; Sirion 200; FEI Co., Eindhoven, Netherlands) and its chemical composition was analyzed using Fourier transform infrared (FTIR) spectra. FTIR spectra were recorded on a VERTEX 70 spectrometer (Bruker Daltonics, Inc., Germany) at 4.0 cm^{-1} resolution.

MBG/SIS-heparin-P28 (MBG/SIS-H-P28): The MBG/SIS scaffolds were immersed in a freshly prepared solution of heparin (1% w/v), 0.5 M N-(3Dimethylaminopropyl)-N'-ethylcarbodiimide hydrochloride (EDC; Sigma-Aldrich, USA), and 0.5 M N-hydroxysuccinimide (NHS; Sigma-Aldrich, USA) in 2-(N-Morpholino) ethanesulfonic acid (MES; Sigma-Aldrich, USA) buffer and were vortexed briefly. After 1 h of incubation at room temperature, the scaffolds were extensively washed with distilled water to remove excess byproducts. Heparin-free modified MBG/SIS scaffold was used as a control group. Next, 3 mg of custom-synthesized peptide P28 (Chinese Peptide Co. Ltd., Hangzhou, China) was dissolved in 100 μL of DI water and loaded onto a MBG/SIS scaffold with defined size and shape (cylinder shape, 5 mm in diameter and 2 mm in height). The actual amount of P28 loaded on the scaffold was evaluated via a previously described method.[24]

Structural Characterization

The pore structure and surface microstructure of the pore wall of pure MBG and MBG/SIS scaffolds were characterized via scanning electron microscopy. Captured images were further processed using Image J software (NIH, USA), and 10 pores per sample (n = 3) were randomly selected for determination of pore size.

The porosity of the prepared scaffolds was measured using the Archimedes' principle following procedures described previously.[29]

The components of MBG, SIS, and MBG/SIS composite scaffolds were characterized using FTIR spectroscopy.

To evaluate the mechanical properties of MBG and MBG/SIS scaffolds, 5 samples per group were subjected to compressive mechanical tests using a computer-controlled universal testing machine (ElectroPuls™ E1000; Instron, Inc., USA) at a cross-head speed of 0.5 mm/min.

In vitro Release of P28 from MBG/SIS-P28 and MBG/SIS-H-P28 Scaffolds

Two types of composite scaffolds were incubated in 1 mL of PBS at 37°C with gentle shaking. At each predetermined time point, 100 μL of supernatant was drawn for examination and replaced with an equal volume of fresh PBS. The samples obtained at each time point were stored at −80°C until the samples for the last time point were collected. Five samples of each composite scaffold were determined by high performance liquid chromatography (HLPC), as previous study.[21]

In vivo Cell Culture

MC3T3-E1 cells were purchased from China Center for Type Culture Collection (Wuhan University) and cultured in basic medium (α-MEM, Gibco) containing 1% penicillin streptomycin (P/S, Gibco) and 10% fetal bovine serum (Gibco, Australia) at 37°C, 5% CO_2, and 95% relative humidity. Osteogenic media contained 100 nM dexamethasone, 10 mM β-glycerophosphate, and 0.05 mM ascorbic acid. In general, cells were cultured in a humidified incubator maintained at 37°C and 5% CO_2. The medium was replenished every 2 d. After the culture in the growth medium reached 80–90% confluence, cells were detached and passaged.

Assessment of Cell Proliferation of MC3T3-E1 on Scaffolds

The MC3T3-E1 cells were seeded at a density of $2*10^5$ cells/well in 24-well plates containing α-MEM supplemented with

10% FBS (Gibco, Australia). After 24 h, the old medium was replaced with fresh medium. A cell proliferation test was performed according to MTT assay instructions (Solarbio, China) on 1D/3D/5D/7D. At each time point, the cells were incubated with MTT assay for 4 h at 37°C away from light. Then, each well was washed thrice with PBS and DMSO was added for 20 min on a horizontal shaker oscillator. Next, 200 μL of solution was drawn from each well and added to a 96-well plate, following which the OD value of each well was measured at 490 nm.

Cell Viability of MC3T3-E1 on Scaffolds

Confocal laser scanning microscopy was used to monitor MC3T3-E1 viability at 3 and 7 d after cell seeding. A total of $2*10^5$ MC3T3-E1 cells were seeded on MBG/SIS, MBG/SIS-P28, and MBG/SIS-H-P28 scaffolds ($1\times1\times0.2$ cm^3) in a 24-well plate. Cells/scaffolds were cultured in growth medium, which was changed every 2 d. Calcein-AM/propidium iodide (PI) double staining (Live/Dead assay; Sigma-Aldrich, USA) was used to quantify cell viability. At each time point, the cells/scaffolds were washed with PBS and incubated in PBS solution containing 2 mM calcein-AM and 4 mM PI for 20 min in the dark. Images from 5 randomly chosen fields per specimen were obtained using a multiphoton confocal fluorescence microscope (Nikon Corporation, Tokyo, Japan) equipped with a digital camera. Image-Pro Plus software 6.0 (Media Cybernetics, Carlsbad, CA, USA) was used to calculate the numbers of live cells. Three specimens from each group (n = 3) yielded 15 images for each time point.

Alkaline Phosphatase Staining and Quantitative Analysis

Alkaline phosphatase (ALP) is an early osteogenic differentiation marker. ALP activity of cells seeded on scaffolds ($1\times1\times0.2$ cm^3) was examined 7 and 14 d after osteogenic induction. A total of $2*10^5$ MC3T3-E1 cells were seeded on MBG/SIS, MBG/SIS-P28, and MBG/SIS-H-P28 scaffolds in a 24-well plate containing osteogenic medium. ALP staining was performed using a BCIP/NBT ALP color development kit (Beyotime Biotechnology, Nanjing, China) following manufacturer's instructions. ALP activity was quantitatively analyzed using a SensoLyte PNPP Alkaline Phosphatase Assay kit (Beyotime Biotechnology, Nanjing, China). Optical density was measured at 405 nm using a microplate reader, and the background intensity of blank wells (ie, scaffold without cells) was subtracted. The ALP activity of samples was calculated via a standard curve. The concentration of double-stranded DNA (dsDNA) in each sample was quantified using a PicoGreen dsDNA Assay Kit (Thermo Fisher Scientific, USA), and ALP activity of each sample was normalized to the dsDNA concentration.

Evaluation of Calcium Nodule Deposition

Alizarin Red S staining was used to observe ECM calcification as described previously.[21] In brief, $2*10^5$ MC3T3-E1 cells seeded on MBG/SIS, MBG/SIS-P28 and MBG/SIS-H-P28 scaffolds ($1\times1\times0.2$ cm^3) were cultured in osteogenic medium for 21 d. At 14 and 21 d, cells/scaffolds were stained according to the manufacturer's protocol for Alizarin red S staining (Beyotime Biotechnology, Nanjing, China). To quantify calcium nodule deposition further, samples were treated with 10% (v/v aqueous solution) cetylpyridinium chloride monohydrate (Sigma-Aldrich, USA) to extract the alizarin red dye. The absorbance of each sample extract was determined spectrophotometrically at 405 nm. The absorbance of the scaffold without cells was subtracted from that of the background. The concentration of alizarin red S in each sample was calculated using the standard curve.

Real-Time PCR

Osteogenesis-related messenger RNA (mRNA) expression levels in MC3T3-E1 cells grown on MBG/SIS, MBG/SIS-P28, and MBG/SIS-H-P28 scaffolds were examined through quantitative real-time reverse transcription polymerase chain reaction (qRT-PCR). Total RNA from $2*10^5$ cells of each sample seeded on scaffolds ($1\times1\times0.2$ cm^3) and cultured in osteogenic medium for 7 and 14 d was isolated using Trizol reagent (Thermo Fisher Scientific, USA). RNA samples were then reverse transcribed into complementary DNA (cDNA) using a PrimeScript reagent Kit (Takara Bio, Shiga, Japan). Real-time PCR was run on a Step One Real-Time PCR system (Applied Biosystems) using a cDNA product template, specific primers, and SYBR Green supermix (Takara Bio, Shiga, Japan) in a total volume of 10 μL. Glyceraldehyde- 3-phosphate-dehydrogenase (GAPDH), a housekeeping gene, was used as a control. Ct values were normalized to the GAPDH gene and the comparative delta Ct method was used to calculate fold induction. Primers for osteogenic genes encoding Ocn, Runx2, ALP, Opn are listed (Table 1).

Animal Experiments

All procedures were approved by the Animal Care and Use Committee at Tongji Medical College, Huazhong University of Science and Technology (IACUC Number: 2353), and in

Table 1

Primer	Forward	Reverse
GAPDH	F5′-GACAAAATGGTGAAGGTCGGT	R5′-GAGGTCAATGAAGGGGTCG
Runx2	F5′-AACTTGCTAACGTGAATGGTC	R5′-TAGCCCACTGAAGAAACTTGG
Opn	F5′-GAGGTGATAGCTTGGCTTACGG	R5′-ACGCTGGGCAACTGGGAT
Ocn	F5′-GAACAGACAAGTCCCACACAG	R5′-TCAGCAGAGTGAGCAGAAAGAT
ALP	F5′-ACCACCACGAGAGTGAACCA	R5′-CGTTGTCTGAGTACCAGTCCC

accordance with the principles of "Guide for the Care and Use of Laboratory Animals". Sprague Dawley rats (30 males, 8 weeks old, 180–200 g) were purchased from the Tongji Experimental Animals Center (Tongji Medical College of HUST). The animals were housed in individual cages at ambient temperature and fed a standard laboratory diet. The rats were anesthetized with chloraldurate (1 mL/kg, intraperitoneal). Surgery was performed under aseptic conditions. A 1.5 cm incision was made in the sagittal direction on the dorsal surface of the cranium. A circular, full-thickness defect with a diameter of 5 mm was then created on the right side of the sagittal suture using a trephine bur to evaluate bone regeneration in the scaffolds in vivo. Scaffolds (Ø5×2mm) were implanted into the defects. Animals were randomly divided into 3 groups as follows: (1) MBG/SIS (n=5); (2) MBG/SIS-P28 (n=5); and (3) MBG/SIS-H-P28 (n=5). At 6 and 12 weeks following surgery, the animals were sacrificed to explant the cranium for micro-computed tomography (CT) examination and histological analysis.

Micro-CT Analysis of Bone Defects

Harvested specimens were explanted and fixed in 4% paraformaldehyde, following which each specimen was clipped with a saw to obtain a size suitable for the scanning container. Afterwards, a micro-CT scanner (Skyscan 1176 X-ray microtomography; Bruker, Germany) was used to evaluate regeneration of the defect on the cranium via scanning at a resolution of 18 μm. A three-dimensional construction of each specimen was observed using NRecon and CTvox softwares. CT-analyzer software was used to analyze percentage bone volume (bone volume/tissue volume, BV/TV) (n = 5).

Histological Assessment

Specimens were decalcified in EDTA (pH 7.0) at 4°C with gentle shaking and the decalcification solution was refreshed regularly. Completely decalcified specimens were embedded in paraffin and sectioned into 5-μm thick slices. For histological analysis, sections were stained with hematoxylin and eosin (H&E). All samples from each group (n = 5) were analyzed using Image-Pro Plus software to assess the new bone fraction in the defect. The new bone fraction was calculated as the new bone area divided by the bone defect area.

Statistical Analysis

All experiments were performed in triplicate unless specified otherwise. All data are expressed as mean±standard deviation. Statistical analysis was performed using the Statistical Package for Social Sciences software (SPSS 16.0). Statistical significance was tested via analysis of variance followed by Tukey's post hoc test. Statistical significance was set at $p < 0.05$ (95% confidence level).

Results

Scaffold Characterization

MBG had a well-ordered channel structure with an approximate pore size of 5 nm, as revealed by TEM analysis (Figure 1A). The resultant hybrid scaffolds (MBG/SIS) exhibited interconnected macropores (200–400 μm) and distinctive micropores (0.2–1.5 μm). SEM analysis showed that the surface of pure MBG scaffolds was relatively smooth, while a thin film was deposited on the surface of composite MBG/SIS scaffolds. Both MBG and MBG/SIS scaffolds possessed high porosity, and interconnected structures with pore sizes ranging from 200 to 400 μm, which was beneficial for cell adhesion, proliferation, and vascular growth (Figure 1B).[32] MBG and MBG/SIS scaffolds exhibited respective porosities of 88%±2% and 86%±3%, which were nearly identical. At higher magnifications, pits caused by freeze-drying were visible on the surface of the scaffold, and these pits further increased the surface area to volume ratio. At higher-magnifications approaching 10,000×, images revealed small, ball-like structures on the surface of the MBG/SIS scaffold, but not on that of the pure MBG scaffold (Figure 1B), which was due to the aggregation of SIS components.

This indicated that SIS can strengthen the mechanical strength of pure MBG scaffold (Figure 1C). The average

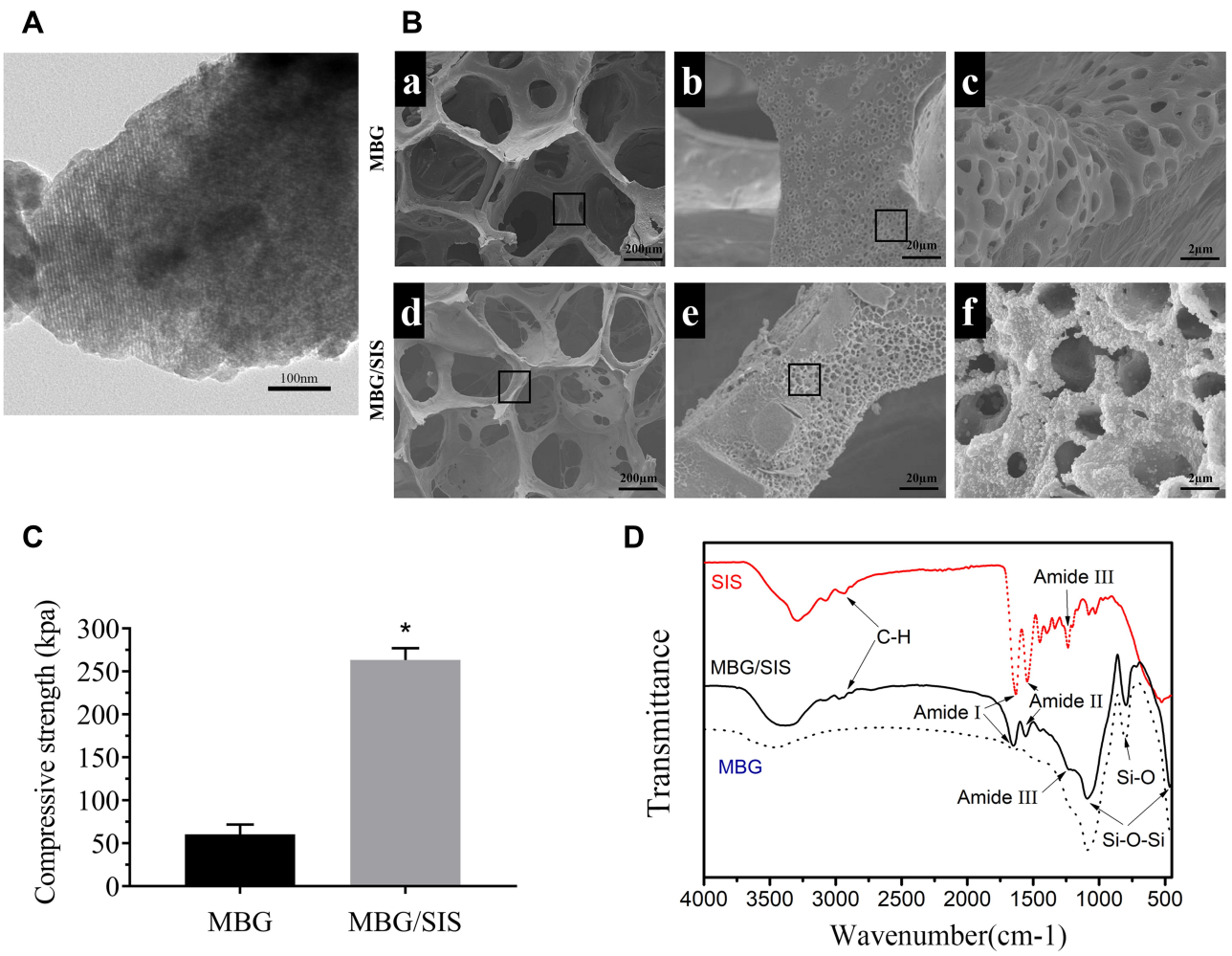

Figure 1 Structural properties of the scaffolds.

Notes: (**A**) TEM image of the prepared MBG powder. MBG have highly ordered mesopore-channel structure. (**B**) SEM images of MBG (a, b and c) and MBG/SIS (d, e and f); (**C**) Compressive strength of MBG and MBG/SIS. (**D**) FTIR spectra of the MBG, SIS, and MBG/SIS. The characteristic peaks of amide groups, alkyl (C–H) groups, and O–Si–O groups are shown on the SIS/MBG spectrum, respectively. It indicates that SIS was successfully incorporated into MBG scaffold. Statistical significance is indicated by *$p < 0.05$ compared to pure MBG group.

Abbreviations: MBG, mesoporous bioactive glass; SIS, small intestinal submucosa; SEM, scanning electron microscopy; TEM, transmission electron microscopy; FTIR, Fourier transform infrared spectroscopy.

compressive strength of pure MBG was 60±4 KPa, whereas the compressive strength of MBG/SIS was 255 ±6 KPa, which was nearly four times higher than that of the pure MBG scaffold ($p < 0.05$).

FTIR analysis of MBG, SIS, and MBG/SIS scaffolds confirmed that the pore wall surfaces of MBG had been coated with SIS (Figure 1D). Characteristic Si–O–Si bands of MBG at 465, 794, and 1089 $cm^{(-1)}$ were clearly evident in the MBG spectrum. Typical transmittance peaks of collagen, including C–H stretching in the range of 2850–3000 $cm^{(-1)}$, C = O stretching at 1650 $cm^{(-1)}$ for amide I, N–H deformation at 1554 $cm^{(-1)}$ for amide II, and N–H deformation at 1232 $cm^{(-1)}$ for amide III bands, respectively, were indicative of SIS conformation.[29]

Release Kinetics of P28 from the Scaffold

P28 loading rates of MBG/SIS and heparin-modified MBG/SIS scaffolds were 90.3 ± 0.4% and 98.5 ±0.3%, respectively. Controlled release of some small molecular peptides or drugs from MBG, due to its ordered mesoporous structure, was envisioned as a ready and feasible design applicable for bone tissue engineering in this study. The release curves of P28 from MBG/SIS-P28 and MBG/SIS-H-P28 scaffolds are presented (Figure 2). These indicate that nearly 90% of P28 was released from MBG/SIS-P28 within 7 d, whereas the release rate of P28 from MBG/SIS-H-P28 was much lower. On the first day, P28 was released from MBG/SIS-H-P28 in a slight burst, whereas it was released in a sustained manner during the days that followed. At the last predetermined point

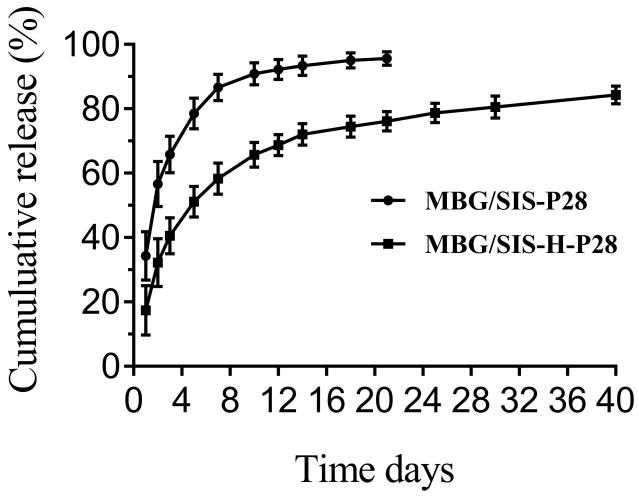

Figure 2 The profiles of P28 peptide released from MBG/SIS-P28 and MBG/SIS-H-P28 scaffolds.
Abbreviations: MBG, mesoporous bioactive glass; SIS, small intestinal submucosa.

in time, 76.3%±2.35% of P28 had been released from MBG/SIS-H-P28 group. Thus, as effective release carriers, MBG/SIS-H-P28 scaffolds were able to achieve high loading and controlled release of P28 due to their closer integration with P28.

Proliferation and Viability of MC3T3-E1 Cells on Scaffolds

Proliferation of MC3T3-E1 cells on the scaffolds was quantified using a MTT kit during culturing (Figure 3A). The content of formazan dye corresponds to the level of active cellular metabolism, which is directly associated with the number of viable cells. The 3 scaffold groups supported cell attachment and proliferation well over a period of 7 d, while the MBG/SIS-H-P28 scaffold

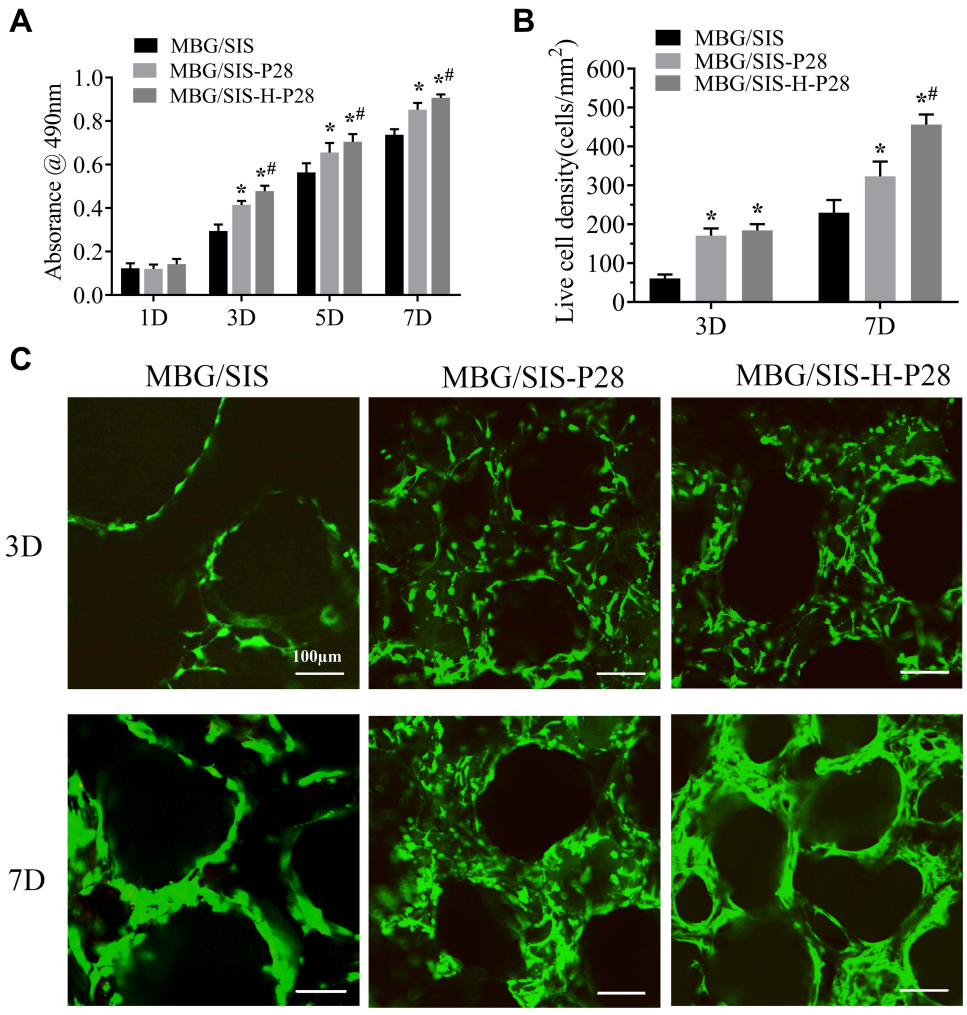

Figure 3 (**A**) The proliferation of MC3T3-E1 cells on MBG/SIS, MBG/SIS-P28, and MBG/SIS-H-P28 scaffolds. (**B**) Cell viability of MC3T3-E1 cells cultured on scaffolds. (**C**) Representative confocal images of cells on scaffolds. Statistical significance is indicated by $^{*}p < 0.05$ compared with MBG/SIS group and $^{\#}p<0.05$ compared with MBG/SIS-P28.
Abbreviations: MBG, mesoporous bioactive glass; SIS, small intestinal submucosa.

sustained higher proliferation compared to control groups. Hence, analysis of cell proliferation revealed that the MBG/SIS-H-P28 scaffold was more conducive to cell adhesion and proliferation, while offering a cell-friendly environment.

Live/Dead assay results of MC3T3-E1 cells in MBG/SIS, MBG/SIS-P28, and MBG/SIS-H-P28 scaffolds are shown in Figure 3B. The results of live cell density trials indicated that MBG/SIS-H-P28 scaffolds supported maximum cell proliferation. Furthermore, the cells in each group attached spontaneously with no dead cells (stained red) being detected during cell culture. The quantitative determination of live cell density in the MBG/SIS, MBG/SIS-P28, and MBG/SIS-H-P28 groups indicated an increase in cell density over time (Figure 3C), further confirming the cell-friendly environment of our scaffolds.

Osteogenic Differentiation Analysis

ALP is a marker of early-stage osteogenic differentiation, and ALP staining results are shown in Figure 4A. Compared with the MBG/SIS group, the MBG/SIS-P28 and MBG/SIS-H-P28 groups significantly promoted ALP production, as shown by a deeper and bluer color response. Moreover, the 7 and 14 d results indicated that reaction color had deepened with the passage of time. Further quantitative analysis of ALP demonstrated that ALP activity in the MBG/SIS-H-P28 group was significantly higher than that in the MBG/SIS and MBG/SIS-P28 groups (Figure 4B).

Alizarin Red S staining was used to analyze ECM calcification as described previously.[33] In brief, MBG/SIS-P28 and MBG/SIS-H-P28 scaffolds showed more mineral formation than the control group, as indicated by a deeper and redder color, which became more obvious at 14 and 21 d (Figure 4C). Further quantitative analysis of ARS (Figure 4D) showed that the OD value in the experimental group was significantly higher than that in the control group.

Osteogenesis-Related Gene Expression Levels

The expression of osteogenesis differentiation genes, *Runx2, ALP, Ocn*, and *Opn*, was measured through qRT-PCR and the results were plotted (Figure 5). The plot revealed that

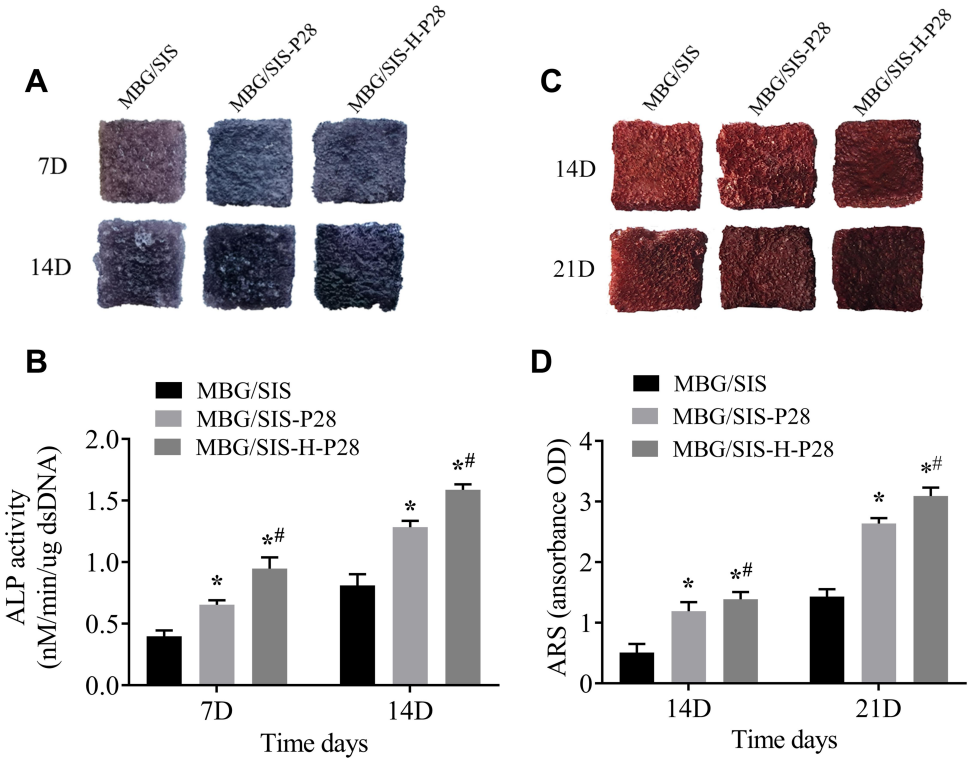

Figure 4 Osteogenic differentiation analysis.

Notes: (**A**) ALP staining of cells on MBG/SIS, MBG/SIS-P28, and MBG/SIS-H-P28 scaffolds at 7 and 14 days. (**B**) The quantification of ALP activity in cells on scaffolds at 7 and 14 days. (**C**) The ARS staining, a marker for minerals deposited by cells on scaffolds at 14 and 21 days. (**D**) The quantification of minerals deposited by cells on scaffolds at 14 and 21 days. Statistical significance is indicated by $^{*}p < 0.05$ compared with MBG/SIS group and $^{\#}p<0.05$ compared with MBG/SIS-P28.

Abbreviations: MBG, mesoporous bioactive glass; SIS, small intestinal submucosa; ALP, alkaline phosphatase; ARS, Alizarin Red S.

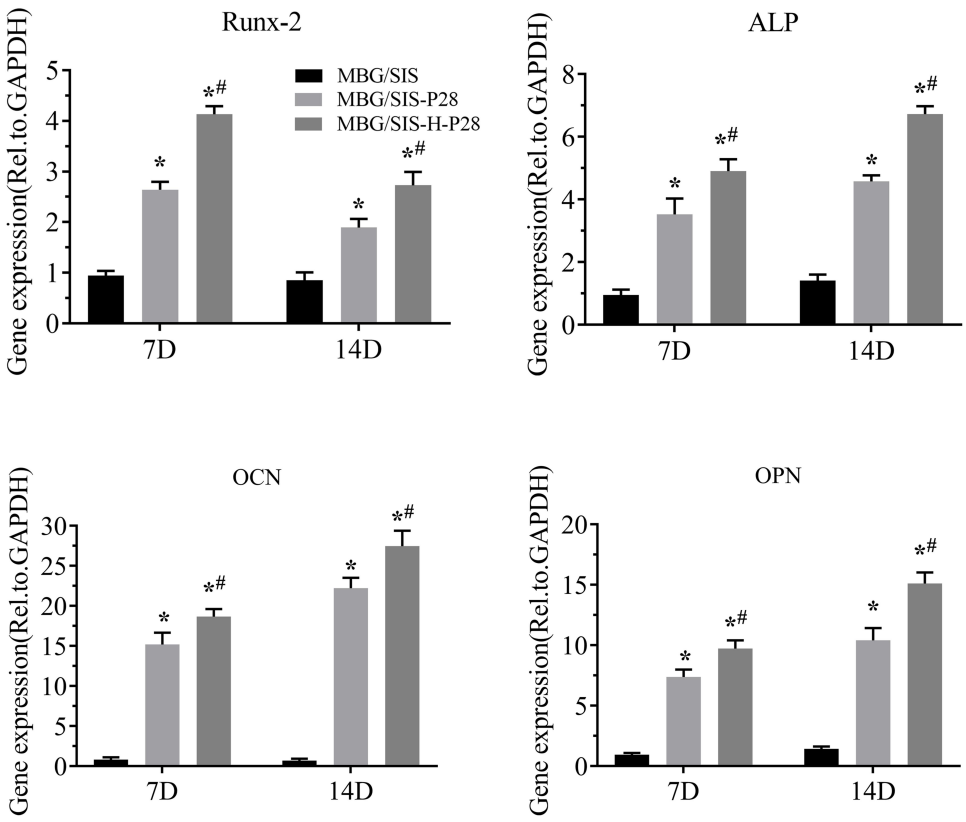

Figure 5 Time course changes in mRNA expression of osteogenic markers, such as Runx-2, ALP, Ocn and Opn in cells on MBG/SIS, MBG/SIS-P28, and MBG/SIS-H-P28 scaffolds after osteogenic induction for 7 and 14 days. Statistical significance is indicated by $^{*}p < 0.05$ compared with MBG/SIS group and $^{\#}p<0.05$ compared with MBG/SIS-P28.
Abbreviations: mRNA, messenger RNA; ALP, alkaline phosphatase; Ocn, osteocalcin; Opn, osteopontin.

MC3T3-E1 cells cultured on MBG/SIS-H-P28 exhibited the highest expression levels of these marker genes on both 7 d and 14 d time points. On day 7, a 2–10 fold increase in *Runx2, ALP*, and *Opn* expression was observed ($p< 0.05$, compared with MBG/SIS or MBG/SIS-P28). *Ocn* was shown to be most responsive to MBG/SIS-H-P28. Its expression was increased by nearly 15-fold. On day 14, a 6–15 fold increase in *ALP* and *Opn* expression and a 25-fold increase in *Ocn* expression was observed in cells cultured on MBG/SIS-H-P28 ($p< 0.05$, compared with MBG/SIS). *Runx2* expression in all 3 groups was higher at 7 d compared with that at 14 d. This may be explained by the fact that transcription factor Runx2 is involved in early osteogenic differentiation. These results suggested that P28 has an excellent effect on osteogenic differentiation, and that heparinized scaffolds showed better osteogenic differentiation due to sustained release of P28.

Animal Experiment Evaluation

Micro-CT images and analyses showed that, at 6 weeks, the volume of newly formed bone was larger in the MBG/SIS-P28 and MBG/SIS-H-P28 groups than in the control group (Figure 6). Furthermore, the defects filled with MBG/SIS-H-P28 scaffolds displayed much greater closure and the highest bone volume fraction (BV/TV%, 20.95 ±1.43%), which was indicative of the most efficient mineralized bone tissue formation. Meanwhile, the bone fraction value increased with time, where, at week 12, the skull defect was almost completely filled with new bone in the MBG/SIS-H-P28 scaffolds, and the value of BV/TV% was up to 32.34±2.13%. Thus, in comparison with the control group, the MBG/SIS-H-P28 group hinted at a higher level of osteogenesis.

Histological and Morphometric Evaluations

H&E stained sections of the 3 groups at 6 and 12 weeks after surgery are shown in Figure 7. At 6 weeks after surgery, the defect in MBG/SIS group was mainly filled with fibrous connective tissue and granulation tissue. On the contrary, the morphological characteristics of active new bone formation were evident in the MBG/SIS-P28

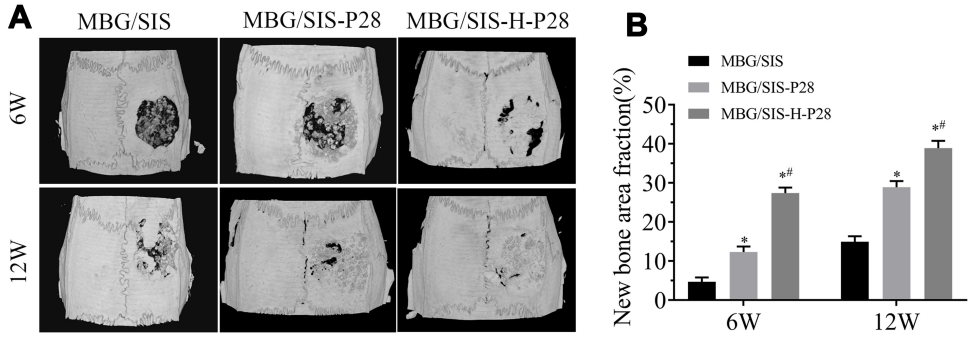

Figure 6 Evaluation of bone formation in calvarial defect through micro-CT.
Notes: (**A**) Representative micro-CT images of calvarial defects treated with MBG/SIS, MBG/SIS-P28, and MBG/SIS-H-P28 scaffolds at 6 and 12weeks. (**B**) Quantitation of BV/TV of new bone in the repaired cranial defect area. Statistical significance is indicated by $^{*}p < 0.05$ compared with MBG/SIS group and $^{\#}p<0.05$ compared with MBG/SIS-P28.
Abbreviations: BV, bone volume; CT, computed tomography; TV, tissue volume.

and MBG/SIS-H-P28 groups: the presence of osteocytes in the lacuna, the formation of new vessels, and a layer of osteoblasts lining the boundaries of the newly formed bone. At 12 weeks after surgery, a small amount of new bone formation was observed in the MBG/SIS group. In contrast, more complete osteointegration was observed in MBG/SIS-P28 and MBG/SIS-H-P28 groups: immature bone was replaced with mature lamellar bone, and the scaffold had completely degraded.

The extent of new bone formation could also be quantified by calculating the percent-area of newly formed bone (Figure 7C). Histological analysis indicated that the MBG/SIS-H-P28 group had the highest new bone area fraction (36.42%±3.77%) compared with that of the MBG/SIS-P28 group (27.53%±2.74%) and the pure MBG/SIS group (13.19%±2.40%). The new bone area fraction increased with time in all groups, especially in the MBG/SIS-H-P28 group. The above results were in accordance with the micro-CT results.

Discussion

Developing an instructive microenvironment similar to that of natural ECM on material-bone surface is critical to direct cell behavior.[32] The current study attempted to dope SIS on MBG scaffolds via polydopamine chemistry, followed by delivery of a BMP2-related peptide to create an osteoinductive microenvironment on the MBG/SIS-bone interface.

Hierarchical porous architecture benefits cell migration, proliferation, and osteogenic differentiation.[34,35] Our study successfully synthesized meso-/macroporous MBG scaffolds using P123 and PU foam as co-templates. The MBG scaffolds can replicate the exquisite and highly interconnected porous structure of cancellous bone. However, high brittleness of the struts of the scaffolds is a serious limitation of hierarchical MBG scaffolds.[36] The compressive strength of an MBG scaffold is around 60 kPa, which is far below the typical range required for cancellous bone (2–12 MPa).[37] Mechanical strength was improved up to 250 kPa by doping the desired thin layer of SIS on the scaffold struts, which maintained high porosity (86±3%) and adequate pore size for tissue in-growth (200–400 μm), good biocompatibility with bone marrow stromal cells, as well as controlled drug delivery and release.

Sustained and controlled release of drugs is an attractive strategy that induces synergistic bone regeneration over a prolonged repair period and reduces the side effects of burst release.[24] Natural ECM contains a wide variety of cytokines and releases growth factors in a spatially and temporally regulated manner due to growth factors such as BMP-2 and BMP-7 participating in specific interactions with the heparan sulfate proteoglycans of ECM.[28] Inspired by the natural delivery mechanisms observed in vivo, the surface of MBG/SIS scaffolds was reinforced with a heparin domain to regulate P28 release.[21] Besides, SIS was efficiently immobilized on MBG scaffolds via the pDA-assisted coating method, which further maintained the control release profile of P28.[38] A mussel-inspired immobilization strategy, pDA chemistry, would provide an easy, safe, and efficient method to deposit proteins and peptides onto polymeric scaffolds.[39–41] The in vitro release curve showed that P28 was initially released from MBG/SIS-H-P28 in a small burst, followed by a slow and sustained release over time. By day 14, 70.3±2.36% of total P28 had been released. This observation may be attributed to two types of affinities: the ionic bond between

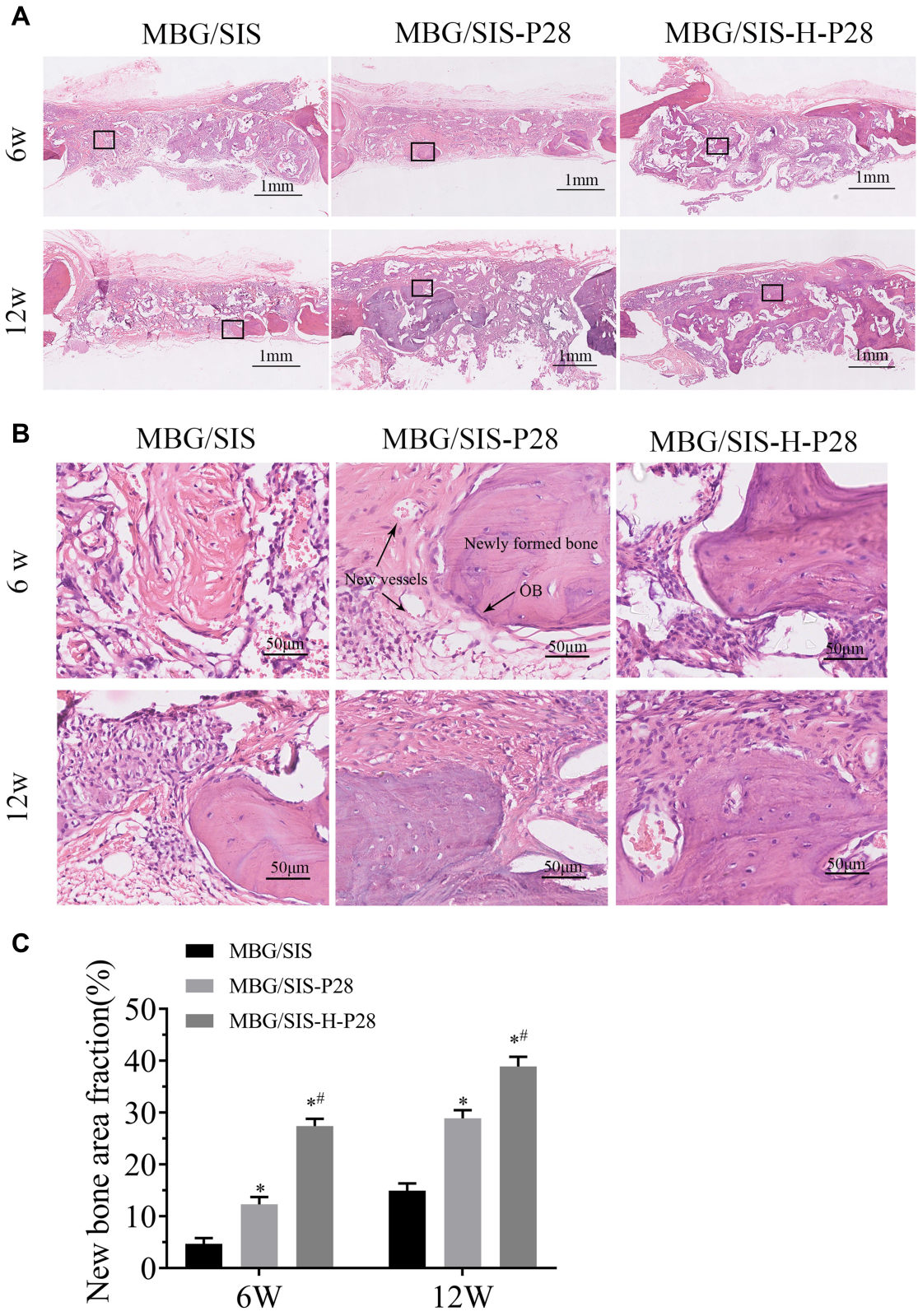

Figure 7 Evaluation of bone regeneration in calvarial defect through histological staining.
Notes: (**A**) Representative H&E staining images of MBG/SIS, MBG/SIS-P28 and MBG/SIS-H-P28 groups at 6 and 12weeks. (**B**) High-magnification image of the black rectangle in A. (**C**) histomorphometry analysis of percentage of new bone area in the rat cranial defect. Statistical significance is indicated by $^{*}p < 0.05$ compared with MBG/SIS group and $^{\#}p<0.05$ compared with MBG/SIS-P28.
Abbreviations: MBG, mesoporous bioactive glass; SIS, small intestinal submucosa; OB, osteoblast cells.

heparin and P28; and an excellent hierarchical porous architecture.[21,42] In the latter situation, controlled pore structure with a pore size equivalent to 200–400 μm led to better regulation of P28 release.[42] The current study revealed that the matrices of MBG/SIS scaffolds reinforced with heparin improved the capacity of sequestering P28, and prolonged the release of P28.

Excellent bony microenvironment of scaffolds is correlated with physical pore structure, and superficial biochemical signals that ensure good cellular penetration and proliferation, as well as nascent tissue development, mass transport, and matrix neovascularization.[35,42] In previous studies, we successfully fabricated porous three-dimensional composite MBG/SIS scaffolds, which displayed superior osteogenesis and angiogenesis via the freeze-drying method.[29] However, inferior biomechanical properties and pore architecture compromise the capability of these scaffolds for bone regeneration.

In the present study, we fabricated MBG/SIS scaffolds using the PU sponge templating method. The method confers higher porosity and more uniform and continuous pore network, which positively affects biologic activity such as cell spreading and transportation of nutrients and oxygen.[43,44] It is expected that the deposition of SIS on the surface of MBG would provide more bioactive factors and a friendly microenvironment to induce desired cellular functions. In this study, MTT assay and Live/dead staining demonstrated that all kinds of scaffolds provide a profitable matrix for cell adhesion and proliferation. Moreover, from 7–14 d, ALP activity and the expression of osteogenic-related genes were up-regulated in cells grown on scaffolds only or scaffolds containing P28. It was reasonable to speculate that the porous MBG/SIS scaffold could inherently guide cells to undergo osteogenic differentiation due to its excellent pore architecture and ability to release ions (Ca, Si and P) and growth factors locally.[29,45,46] Moreover, treatment with P28 resulted in an even higher proliferation and osteoblastic activity and a greater potential to accelerate new bone formation compared with the scaffold alone. In accordance with a previous study, P28, the novel BMP2-mimicking peptide, successfully induced osteogenic differentiation.[24] Moreover, a controllable delivery system of MBG/SIS-H-P28 was designed to overcome its burst release and short-life, and to improve the biological efficacy of P28. Compared with MBG/SIS or MBG/SIS-P28, MBG/SIS-H-P28 exerted a higher stimulatory effect on proliferation and osteogenic differentiation of MC3T3-E1 cells, which is suggestive of the synergistic effect of the controlled release of P28 on osteogenesis activity.

A rat cranial bone defect experiment was performed to evaluate osteogenic capabilities of composite biomaterials in vivo. The results showed that compared to MBG/SIS scaffolds, the MBG/SIS-H-P28 and MBG/SIS-P28 scaffolds enhanced bone regeneration, and that MBG/SIS-H-P28 induced the highest bone regeneration, indicating that controlled release of P28 improved bone regeneration. Micro-CT analysis showed that higher BV/TV ratio, representing new bone fraction, was observed in the MBG/SIS-H-P28 group than in the other groups at weeks 6 and 12. The results of the histological analysis were consistent with the micro-CT findings. Thus, P28 released from MBG/SIS-H-P28 exhibited strong osteoinductive bioactivity in vivo, and accelerated the healing of critical-sized bone defects. Considered together, these results indicated that MBG/SIS-H-P28 scaffolds provide an ideal platform for P28 delivery and a bony environment conducive to bone regeneration.

In summation, the current study attributes the high bone regeneration ability of MBG/SIS-H-P28 to the following criteria: Firstly, the physical features of the MBG/SIS hierarchical porous architecture exert a positive effect on the osteogenic differentiation of stem cells. Secondly, MBG/SIS inherently releases multiple bioactive components, such as VEGF or bFGF, and chemical ions, such as Si or Ca, stimulating cell proliferation and differentiation, which leads to further tissue regeneration. Thirdly, SIS coating endows MBG with a functional interface to regulate cell-matrix interactions and osteogenic commitment of stem cells. Lastly, the ECM-inspired delivery system, MBG/SIS-H-P28, improved P28 loading efficacy, facilitated its controlled release, and promoted specific interactions between P28 and cells.

Conclusion

The current study utilized PU foam templating and pDA chemistry method to develop a novel tissue-derived ECM scaffold, MBG/SIS, with a hierarchical and interconnected porous architecture. To mimic the environment of natural bone matrix an ECM-inspired delivery system was constructed by coupling a BMP2-related peptide, P28, to heparinized MBG/SIS scaffolds (MBG/SIS-H-P28). MBG/SIS-H-P28 significantly improved the loading efficiency and release kinetics of P28, and regulated cell responses. An in vitro study revealed that MBG/SIS-H-P28 not only provides biological cues needed for cell proliferation and adhesion, but also elevates ALP activity and expression of the osteogenic genes, *Runx-2, OCN,*

OPN, and *ALP*. An in vivo study indicated that MBG/SIS-H-P28 scaffolds exhibit a much stronger ability to stimulate bone regeneration.

Funding

This research was financially supported by the National Natural Science Foundation of China (grant numbers 81902219, 81672158 and 81873999) and the National Key R&D Program of China (2016YFC1100100).

Disclosure

No competing financial interests exist. The authors report no conflicts of interest for this work.

References

1. Salgado CL, Teixeira BIB, Monteiro FJM. Biomimetic composite scaffold with phosphoserine signaling for bone tissue engineering application. *Front Bioeng Biotechnol*. 2019;7:206. doi:10.3389/fbioe.2019.00206
2. Zhang J, Wu H, He F, Wu T, Zhou L, Ye J. Concentration-dependent osteogenic and angiogenic biological performances of calcium phosphate cement modified with copper ions. *Mater Sci Eng C Mater Biol Appl*. 2019;99:1199–1212. doi:10.1016/j.msec.2019.02.042
3. Shao H, Ke X, Liu A, et al. Bone regeneration in 3D printing bioactive ceramic scaffolds with improved tissue/material interface pore architecture in thin-wall bone defect. *Biofabrication*. 2017;9(2):025003. doi:10.1088/1758-5090/aa663c
4. Ou Q, Miao Y, Yang F, Lin X, Zhang LM, Wang Y. Zein/gelatin/nanohydroxyapatite nanofibrous scaffolds are biocompatible and promote osteogenic differentiation of human periodontal ligament stem cells. *Biomater Sci*. 2019;7(5):1973–1983. doi:10.1039/C8BM01653D
5. He X, Liu Y, Tan Y, et al. Rubidium-containing mesoporous bioactive glass scaffolds support angiogenesis, osteogenesis and antibacterial activity. *Mater Sci Eng C Mater Biol Appl*. 2019;105:110155. doi:10.1016/j.msec.2019.110155
6. Qi X, Wang H, Zhang Y, et al. Mesoporous bioactive glass-coated 3D printed borosilicate bioactive glass scaffolds for improving repair of bone defects. *Int J Biol Sci*. 2018;14(4):471–484. doi:10.7150/ijbs.23872
7. Bari A, Bloise N, Fiorilli S, et al. Copper-containing mesoporous bioactive glass nanoparticles as multifunctional agent for bone regeneration. *Acta Biomater*. 2017;55:493–504.
8. Wang X, Liu Q, Chen W, Liu L. FGF adsorbed mesoporous bioactive glass with larger pores in enhancing bone tissue engineering. *J Mater Sci Mater Med*. 2019;30(4):48. doi:10.1007/s10856-019-6252-8
9. Chandrasekaran A, Novajra G, Carmagnola I, et al. Physico-chemical and biological studies on three-dimensional porous silk/spray-dried mesoporous bioactive glass scaffolds. *Ceram Int*. 2016;42(12):13761–13772. doi:10.1016/j.ceramint.2016.05.176
10. Hatton J, Davis GR, Mourad AI, Cherupurakal N, Hill RG, Mohsin S. Fabrication of porous bone scaffolds using alginate and bioactive glass. *J Funct Biomater*. 2019;10.
11. Higa K, Kitamura N, Kurokawa T, et al. Fundamental biomaterial properties of tough glycosaminoglycan-containing double network hydrogels newly developed using the molecular stent method. *Acta Biomater*. 2016;43:38–49. doi:10.1016/j.actbio.2016.07.023
12. Pereira AM, Machado R, da Costa A, et al. Silk-based biomaterials functionalized with fibronectin type II promotes cell adhesion. *Acta Biomater*. 2017;47:50–59. doi:10.1016/j.actbio.2016.10.002
13. Zhang X, Li Y, Chen YE, Chen J, Ma PX. Cell-free 3D scaffold with two-stage delivery of miRNA-26a to regenerate critical-sized bone defects. *Nat Commun*. 2016;7(1):10376. doi:10.1038/ncomms10376
14. AhmedC M, ffrench-Constant C. Extracellular matrix regulation of stem cell behavior. *Curr Stem Cell Rep*. 2016;2(3):197–206. doi:10.1007/s40778-016-0056-2
15. Lin X, Robinson M, Petrie T, Spandler V, Boyd WD, Sondergaard CS. Small intestinal submucosa-derived extracellular matrix bioscaffold significantly enhances angiogenic factor secretion from human mesenchymal stromal cells. *Stem Cell Res Ther*. 2015;6(1):164. doi:10.1186/s13287-015-0165-3
16. Wang W, Zhang X, Chao NN, et al. Preparation and characterization of pro-angiogenic gel derived from small intestinal submucosa. *Acta Biomater*. 2016;29:135–148. doi:10.1016/j.actbio.2015.10.013
17. Jiang W, Zhang J, Lv X, et al. Use of small intestinal submucosal and acellular dermal matrix grafts in giant omphaloceles in neonates and a rabbit abdominal wall defect model. *J Pediatr Surg*. 2016;51(3):368–373. doi:10.1016/j.jpedsurg.2015.08.005
18. Liang R, Yang G, Kim KE, et al. Positive effects of an extracellular matrix hydrogel on rat anterior cruciate ligament fibroblast proliferation and collagen mRNA expression. *J Orthop Translat*. 2015;3(3):114–122. doi:10.1016/j.jot.2015.05.001
19. Rong JJ, Sang HF, Qian AM, Meng QY, Zhao TJ, Li XQ. Biocompatibility of porcine small intestinal submucosa and rat endothelial progenitor cells in vitro. *Int J Clin Exp Pathol*. 2015;8:1282–1291.
20. Ji Y, Zhou J, Sun T, et al. Diverse preparation methods for small intestinal submucosa (SIS): decellularization, components, and structure. *J Biomed Mater Res A*. 2019;107:689–697.
21. Sun T, Liu M, Yao S, et al. Guided osteoporotic bone regeneration with composite scaffolds of mineralized ECM/heparin membrane loaded with BMP2-related peptide. *Int J Nanomedicine*. 2018;13:791–804. doi:10.2147/IJN.S152698
22. Kang Y, Kim S, Khademhosseini A, Yang Y. Creation of bony microenvironment with CaP and cell-derived ECM to enhance human bone-marrow MSC behavior and delivery of BMP-2. *Biomaterials*. 2011;32(26):6119–6130. doi:10.1016/j.biomaterials.2011.05.015
23. Zhang X, Yu Q, Wang YA, Zhao J. Dose reduction of bone morphogenetic protein-2 for bone regeneration using a delivery system based on lyophilization with trehalose. *Int J Nanomedicine*. 2018;13:403–414. doi:10.2147/IJN.S150875
24. Sun T, Qu Y, Cui W, et al. Evaluation of osteogenic inductivity of a novel BMP2-mimicking peptide P28 and P28-containing bone composite. *J Biomed Mater Res A*. 2018;106(1):210–220. doi:10.1002/jbm.a.36228
25. James AW, LaChaud G, Shen J, et al. A review of the clinical side effects of bone morphogenetic protein-2. *Tissue Eng Part B Rev*. 2016;22(4):284–297. doi:10.1089/ten.teb.2015.0357
26. Jiang T, Yu X, Carbone EJ, Nelson C, Kan HM, Lo KW. Poly aspartic acid peptide-linked PLGA based nanoscale particles: potential for bone-targeting drug delivery applications. *Int J Pharm*. 2014;475(1–2):547–557. doi:10.1016/j.ijpharm.2014.08.067
27. Kobuke S, Suzuki S, Hoshino H, Haruyama N, Nishimura F, Shiba H. Relationship between length variations in Ser/Asp-rich repeats in phosphophoryn and in vitro precipitation of calcium phosphate. *Arch Oral Biol*. 2015;60(9):1263–1272. doi:10.1016/j.archoralbio.2015.05.013
28. Martino MM, Briquez PS, Maruyama K, Hubbell JA. Extracellular matrix-inspired growth factor delivery systems for bone regeneration. *Adv Drug Deliv Rev*. 2015;94:41–52. doi:10.1016/j.addr.2015.04.007
29. Sun T, Liu M, Yao S, et al. Biomimetic composite scaffold containing small intestinal submucosa and mesoporous bioactive glass exhibits high osteogenic and angiogenic capacity. *Tissue Eng Part A*. 2018;24(13–14):1044–1056. doi:10.1089/ten.tea.2017.0398
30. Pan H, Zheng Q, Guo X, Wu Y, Wu B. Polydopamine-assisted BMP-2-derived peptides immobilization on biomimetic copolymer scaffold for enhanced bone induction in vitro and in vivo. *Colloids Surf B Biointerfaces*. 2016;142:1–9. doi:10.1016/j.colsurfb.2016.01.060
31. Sun T, Yao S, Liu M, et al. Composite scaffolds of mineralized natural extracellular matrix on true bone ceramic induce bone regeneration through Smad1/5/8 and ERK1/2 pathways. *Tissue Eng Part A*. 2018;24:502–515.

32. Da L, Gong M, Chen A, et al. Composite elastomeric polyurethane scaffolds incorporating small intestinal submucosa for soft tissue engineering. *Acta Biomater*. 2017;59:45–57. doi:10.1016/j.actbio.2017.05.041
33. Sun T, Zhou K, Liu M, et al. Loading of BMP-2-related peptide onto three-dimensional nano-hydroxyapatite scaffolds accelerates mineralization in critical-sized cranial bone defects. *J Tissue Eng Regen Med*. 2018;12(4):864–877. doi:10.1002/term.2371
34. Tang W, Lin D, Yu Y, et al. Bioinspired trimodal macro/micro/nano-porous scaffolds loading rhBMP-2 for complete regeneration of critical size bone defect. *Acta Biomater*. 2016;32:309–323. doi:10.1016/j.actbio.2015.12.006
35. Carvalho MS, Silva JC, Udangawa RN, et al. Co-culture cell-derived extracellular matrix loaded electrospun microfibrous scaffolds for bone tissue engineering. *Mater Sci Eng C Mater Biol Appl*. 2019;99:479–490. doi:10.1016/j.msec.2019.01.127
36. Wu C, Zhou Y, Xu M, et al. Copper-containing mesoporous bioactive glass scaffolds with multifunctional properties of angiogenesis capacity, osteostimulation and antibacterial activity. *Biomaterials*. 2013;34(2):422–433. doi:10.1016/j.biomaterials.2012.09.066
37. Ciraldo FE, Liverani L, Gritsch L, Goldmann WH, Boccaccini AR. Synthesis and characterization of silver-doped mesoporous bioactive glass and its applications in conjunction with electrospinning. *Materials (Basel)*. 2018;11.
38. Wang X, Chen Z, Zhou B, et al. Cell-sheet-derived ECM coatings and their effects on BMSCs responses. *ACS Appl Mater Interfaces*. 2018;10(14):11508–11518. doi:10.1021/acsami.7b19718
39. Mrowczynski R. Polydopamine-based multifunctional (nano)materials for cancer therapy. *ACS Appl Mater Interfaces*. 2018;10(9):7541–7561. doi:10.1021/acsami.7b08392
40. Kao CT, Chen YJ, Ng HY, et al. Surface modification of calcium silicate via mussel-inspired polydopamine and effective adsorption of extracellular matrix to promote osteogenesis differentiation for bone tissue engineering. *Materials (Basel)*. 2018;11.
41. Wang H, Lin C, Zhang X, Lin K, Wang X, Shen SG. Mussel-inspired polydopamine coating: a general strategy to enhance osteogenic differentiation and osseointegration for diverse implants. *ACS Appl Mater Interfaces*. 2019;11(7):7615–7625. doi:10.1021/acsami.8b21558
42. Chen G, Sun Y, Lu F, et al. A three-dimensional (3D) printed biomimetic hierarchical scaffold with a covalent modular release system for osteogenesis. *Mater Sci Eng C Mater Biol Appl*. 2019;104:109842. doi:10.1016/j.msec.2019.109842
43. Wu C, Zhang Y, Zhu Y, Friis T, Xiao Y. Structure-property relationships of silk-modified mesoporous bioglass scaffolds. *Biomaterials*. 2010;31(13):3429–3438. doi:10.1016/j.biomaterials.2010.01.061
44. Wang X, Lin M, Kang Y. Engineering porous beta-tricalcium phosphate (beta-TCP) scaffolds with multiple channels to promote cell migration, proliferation, and angiogenesis. *ACS Appl Mater Interfaces*. 2019;11(9):9223–9232. doi:10.1021/acsami.8b22041
45. Baino F, Fiorilli S, Vitale-Brovarone C. Bioactive glass-based materials with hierarchical porosity for medical applications: review of recent advances. *Acta Biomater*. 2016;42:18–32. doi:10.1016/j.actbio.2016.06.033
46. Li M, Zhang C, Cheng M, Gu Q, Zhao J. Small intestinal submucosa: a potential osteoconductive and osteoinductive biomaterial for bone tissue engineering. *Mater Sci Eng C Mater Biol Appl*. 2017;75:149–156. doi:10.1016/j.msec.2017.02.042

International Journal of Nanomedicine Dovepress

Publish your work in this journal

The International Journal of Nanomedicine is an international, peer-reviewed journal focusing on the application of nanotechnology in diagnostics, therapeutics, and drug delivery systems throughout the biomedical field. This journal is indexed on PubMed Central, MedLine, CAS, SciSearch®, Current Contents®/Clinical Medicine, Journal Citation Reports/Science Edition, EMBase, Scopus and the Elsevier Bibliographic databases. The manuscript management system is completely online and includes a very quick and fair peer-review system, which is all easy to use. Visit http://www.dovepress.com/testimonials.php to read real quotes from published authors.

Submit your manuscript here: https://www.dovepress.com/international-journal-of-nanomedicine-journal